ACS Catalysis

Research Article

Cite This: ACS Catal. 2019, 9, 5496−5502

pubs.acs.org/acscatalysis

Plasma-Modified Dendritic Cu Catalyst for CO_2 Electroreduction

Fabian Scholten,[†,‡] Ilya Sinev,[†] Miguel Bernal,[†] and Beatriz Roldan Cuenya*[,‡]

[†]Department of Physics, Ruhr-University Bochum, Bochum 44780, Germany

[‡]Interface Science Department, Fritz-Haber Institute of the Max Planck Society, Berlin 14195, Germany

Supporting Information

ABSTRACT: Efficient and active catalysts with high selectivity for hydrocarbons and other valuable chemicals during stable operation are crucial. We have taken advantage of low-pressure oxygen plasmas to modify dendritic Cu catalysts and were able to achieve enhanced selectivity toward C_2 and C_3 products. Utilizing operando spectroscopic methods such as X-ray absorption fine-structure spectroscopy (XAFS) and quasi in situ X-ray photoelectron spectroscopy (XPS), we observed that the initial presence of oxides in these catalysts before the reaction plays an inferior role in determining their catalytic performance as compared to the overall catalyst morphology. This is assigned to the poor stability of the Cu_xO species in these materials under the conditions of electrocatalytic conversion of CO_2 (CO_2RR). Our findings shed light into the strong structure/chemical state-selectivity correlation in CO_2RR and open venues for the rational design of more effective catalysts through plasma pretreatments.

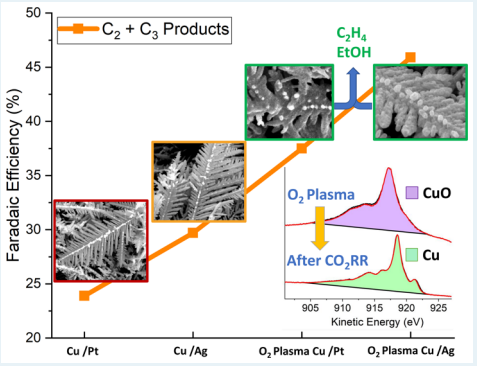

KEYWORDS: *CO_2 electro-reduction, Cu dendrites, XPS, XAFS, oxide-derived Cu*

INTRODUCTION

Due to the rapid advance in technology and simultaneous drastic increase of the overall population, the demand for energy is a concern of general societal interest. A promising strategy toward sustainable energy is the use of electricity derived from renewable energy sources to drive the electrocatalytic conversion of CO_2 (CO_2RR) into valuable chemicals and fuels[1] that can be subsequently used as feedstock for the chemical industry or as energy storage technology.[2,3]

Among the various catalysts studied so far,[4−6] copper has been shown to have the unique ability to produce hydrocarbons, especially C_2 and C_3 compounds,[4,7] which is due to its moderate binding energy for CO[8] and optimum H binding.[9] The downside is that, unlike other metals such as Ag[10−12] and Au[13,14] or Sn[5,15] and Pb[15] that display high selectivity for CO or $HCOO^-$, respectively, in the case of copper, it is difficult to target the desired products.[1,8,16,17] Various electrode parameters such as composition,[18−20] surface morphology and structure,[21] chemical state,[21−23] prefunctionalization[21,23] or electrolyte characteristics such as its composition[21,23−28] and pH,[29] as well as thermodynamic parameters like temperature[30] and pressure,[30,31] were found to drastically affect the catalysts performance. Nevertheless, a detailed picture of how the reaction takes place in a number of active Cu-based catalysts is missing.

Nanostructured catalysts have proven to outperform bulk materials[21,32] in many aspects of CO_2RR. For instance, a superior catalytic performance with respect to ethylene production has been observed for Cu nanocubes and attributed to the presence of subsurface oxygen/Cu^+ species[21,23] and Cu(100) facets.[21,22,33] Additionally, kinetic transport limitations can be overcome by using high surface area nanoporous catalysts such as copper dendrites, which can be operated in a three-phase (gas/solid/liquid)[32,34] flow cell setup with an already demonstrated 63% faradaic efficiency (FE) for ethylene at current densities of up to 750 mA/cm^2.[35] Other materials tested in similar flow cells were also found to provide excellent C_{2+} selectivity at high current densities.[32,35,36]

The exceptional C_2H_4 selectivity previously reported for dendritic catalysts[32,36] was also shared by oxide-derived (OD) catalysts, which also displayed an increased selectivity for multicarbon products while suppressing methane formation.[23,28,37] Although a correlation between the presence of Cu(I) species and subsurface oxygen in Cu-based catalysts and their selectivity for C2−C3 products has been theoretically predicted[32,33] and experimentally demonstrated by several groups,[19,25,34,35] their small content and difficult stabilization makes their detection challenging and still controversial in the literature. It requires a synergistic combination of surface and bulk-sensitive in situ and operando methods able to probe surface and subsurface regions of the catalysts with high sensitivity. Furthermore, the morphology of the catalyst,[19,27,36] initial composition,[19,37,38] pretreatment for the generation of the oxides,[20] Cu particle support,[26,39] and Cu−electrolyte interactions[33,40] are key parameters for the stabilization of Cu(I). While Cu(I) is not very stable on smooth surfaces, it can be

Received: January 31, 2019
Revised: March 22, 2019
Published: April 30, 2019

DOI: 10.1021/acscatal.9b00483
ACS Catal. 2019, 9, 5496−5502

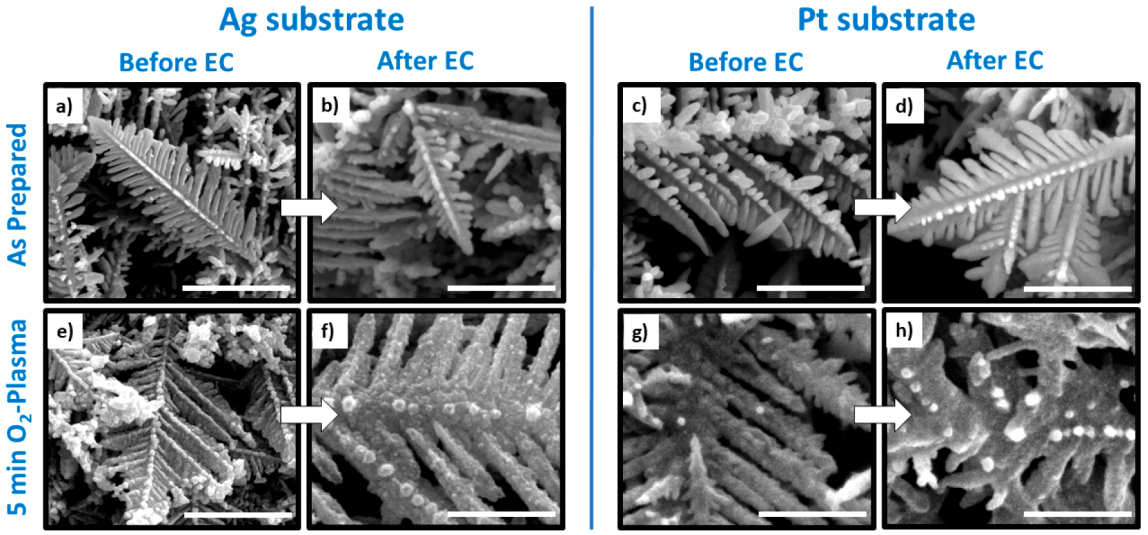

Figure 1. SEM images of Cu dendrites deposited on an Ag-foil (a, b, e, f) and Pt-foil (c, d, g, h) acquired before and after CO_2RR at −1.0 V vs RHE for the untreated (a−d) and 5 min O_2-plasma treated (e−h) samples. The scale bars correspond to 2 μm.

stabilized at preoxidized Cu cube/Cu foil interfaces or as CuI in iodine-pretreated surfaces, in boron-doped copper[34] or in copper−nitrate-based catalysts.[35]

To date, no detailed in situ or operando study is available on dendritic catalysts to shed light into the possible transformations in their morphology/structure and chemical state under CO_2RR conditions and to distinguish the possible influence of such parameters in the selectivity trends previously reported.

In this work, we report that, although Cu(I) species have been demonstrated to be advantageous for the increased yield of C2−C3 products, the stabilization of such species requires a delicate interplay among the morphology of the Cu catalysts and its interaction with the environment, such as the support and electrolyte. In the present case, our quasi in situ X-ray photoelectron spectroscopy (XPS) and operando X-ray absorption fine-structure spectroscopy (XAFS) data revealed that Cu(I) species are not stable on the large (micrometer structures) dendritic Cu catalysts supported on Ag and Pt and that the selectivity trends observed can be exclusively assigned to their morphology and the contribution from exposed regions of the respective underlying supports (Ag or Pt). In this case, and contrary to our previous observations for smaller Cu cubes on Cu, Cu(I) species are not stable at the Cu_xO/Ag or Pt interfaces, which might be explained on the basis of the lower stability of AgOx and PtOx species and the much lower contact area and interaction with the support of the Cu dendrites as compared, for example, to our former O_2-plasma treated Cu cubes grown on a Cu foil.[1,2]

EXPERIMENTAL SECTION

Synthesis. Cu dendrites were grown on Ag and Pt foils (99.9999%, Advent Research Materials) via electrodeposition at a constant potential of $U_{applied}$ = −1.25 V vs RHE from an aqueous solution containing 0.05 M $CuSO_4$ (99.9995%, Sigma-Aldrich) at a pH of 2−3 by the addition of H_2SO_4 (adapted from ref 32). Oxygen plasma treatments were carried out for 1 and 5 min at a pressure of 250 mTorr with a power of 20 W (Plasma Prep III, SPI Supplies). Prior to use, the Ag foils were etched for 2 min in an aqueous 0.5 M HNO_3 solution while the Pt foils were etched for 2 min in 1 M H_2SO_4 to remove metal contaminations, which are known to poison Cu during CO_2RR.[39,40]

Electrochemical Characterization. The reactions were carried out in a customized H-type glass cell using a conventional three electrode setup. A platinum mesh and a leak-free Ag/AgCl electrode (LF-1, Innovative Instruments, Inc.) were used as counter and reference electrode. The electrolyte employed was 0.1 M $KHCO_3$ (ACS reagent 99.7%, Sigma-Aldrich). To be able to compare the results with the literature, measurements were also conducted in the absence of the O_2-plasma pretreatment. Prior to usage, the electrolyte was treated with Chelex (Bio-Rad Laboratories Inc.) to remove trace metal impurities.[40,41] Before introducing the working electrode into the cell, the electrolyte was purged with CO_2 gas (99.95%, Air Liquide) for 30 min until a pH of 6.8 was reached. The reaction was investigated at different potentials using the chronoamperometry method. Gas products from the cell were injected online every 16 min into a gas chromatograph (GC, Shimadzu 2014; HayeSepQ + HayeSepR column; flame ionization detector (FID) and thermal conductivity detector (TCD)) while the liquid products were detected after 1.5 h of reaction using a liquid chromatograph (HPLC Shimadzu; NUCLEOGEL SUGAR 810 column; refractive index detector (RID)).

Quasi in Situ X-ray Photoelectron Spectroscopy. Quasi in situ XPS measurements were performed directly after electrochemistry without exposing the sample to air by transferring it from the electrochemical cell (EC-Cell) to the adjacent XPS chamber in ultrahigh vacuum (UHV). Before UHV transfer, the sample was rinsed within the electrochemical cell with 10 mL of deionized water (R = 18.2 MΩ), which was bubbled with N_2 (99.999%, Air Liquide) for 45 min prior to usage. Figure S1 shows the experimental setup. For the XPS measurements, a commercial Phoibos100 analyzer (SPECS GmbH, E_{pass} = 15 eV) and XR50 (SPECS GmbH) X-ray source were employed. For our study, the Al anode (P_{source} = 300 W) was used to measure all but the Cu-Auger spectra. A Mg anode (P_{source} = 250 W) was utilized to avoid an overlap with the Ag 3p region in the case of the Cu samples grown on the Ag substrate. The Cu $2p_{3/2}$ peak corresponding to CuO (E_{bin} = 933.11 eV)[42] was used to align the spectra for the samples containing CuO, and the binding energy of Cu/Cu_2O (E_{bin} = 932.67 eV)[42] was used for the samples not showing any CuO. The electrochemical

DOI: 10.1021/acscatal.9b00483
ACS Catal. 2019, 9, 5496−5502

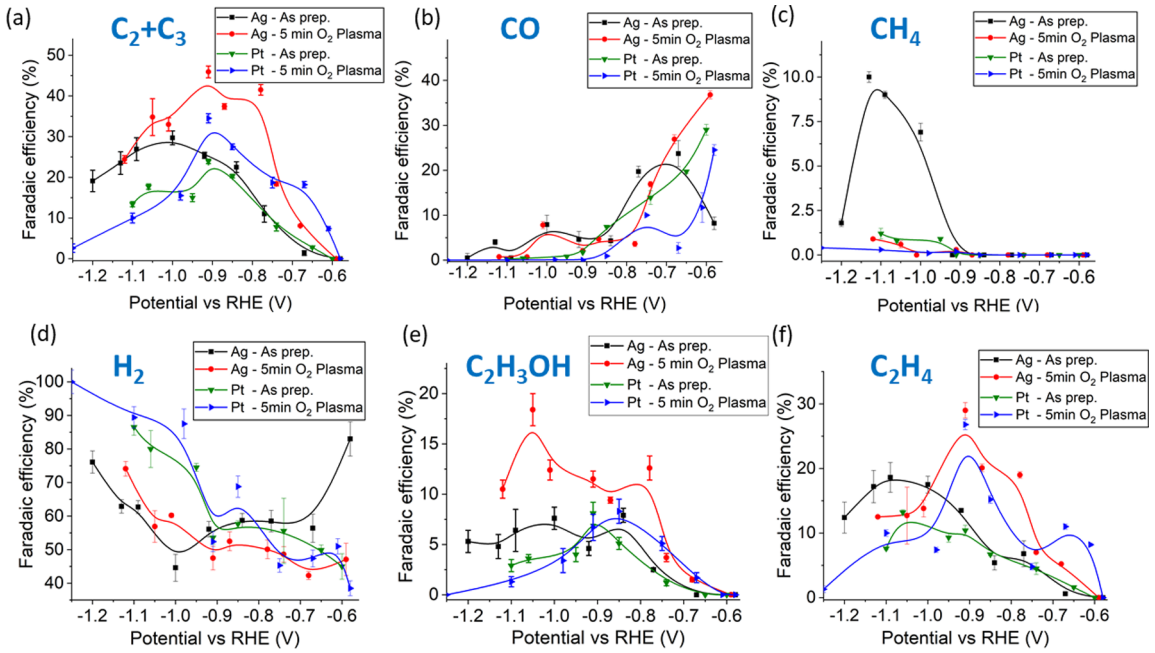

Figure 2. (a) Combined CO_2RR faradaic efficiency for $C_2 + C_3$ products and individual faradaic efficiencies for (b) CO, (c) CH_4, (d) H_2, (e) ethanol, and (f) C_2H_4 from Cu dendrites grown on Ag (black and red curves) and Pt (green and blue curves) substrates as a function of the potential in 0.1 M $KHCO_3$. Data from the as prepared (untreated) and 5 min O_2-plasma treated samples are shown. Solid lines are a guide for the eye.

measurements were carried out using an Autolab potentiostat (PGSTAT 302N).

Scanning Electron Microscopy. Scanning electron microscopy (SEM) measurements were performed using a Quanta 200 FEG microscope from FEI with a field emitter as electron source (10 kV). To acquire the images, a secondary electron detector (Everhart Thornley) was employed. The EDX measurements were performed with a separate liquid-N_2-cooled detector (10 kV).

X-ray Absorption Fine-Structure Spectroscopy. The XAFS measurements were performed at the undulator beamline P65 of the PETRA III storage ring operating at 6 GeV in top-up mode. For the energy scan, a Si(111) monochromator was used with 60% detuning to reject higher harmonics. The experiments were performed in fluorescence mode at the Cu−K edge (8989 eV) at an angle of 15° using a Passivated Implanted Planar Silicon (PIPS) detector. For each sample, multiple identical spectra were acquired before and under operando conditions and averaged to improve the signal-to-noise ratio. Initial processing of the data was performed in Athena.[43] The spectra have also been corrected for self-absorption using the algorithms implemented within Athena,[44] so that the edges and the edge step size of the merged spectra and our measured reference spectra were aligned. Extended X-ray absorption fine-structure spectroscopy (EXAFS) analysis was conducted in Artemis using the FEFF6 code[43] to extract the coordination numbers (CN), interatomic distances, and disorder parameters. S_0, the amplitude reduction factor accounting for many body effects, was determined by fitting our measured reference with a fixed coordination number of $N = 12$ for the Cu−Cu coordination. Linear combination fitting of the X-ray absorption near-edge spectroscopy (XANES) data was done using Athena.

In order to perform the operando measurements, a customized three electrode electrochemical cell including a leak-free Ag/AgCl reference and a Pt mesh counter electrode was used. The electrolyte was an aqueous solution of 0.1 M $KHCO_3$.

RESULTS AND DISCUSSION

Figure 1 shows typical SEM images obtained on our Cu dendrite catalysts deposited on Ag and Pt foils before and after a 5 min O_2-plasma treatment and subsequent CO_2RR. It is important to note that, due to the evolving hydrogen bubbles during the Cu dendrite electrodeposition process, parts of the different substrates are not completely covered with copper dendrites after electrodeposition (see Figure S2), and consequently, the substrates may serve as active cocatalyst supports during the CO_2RR.

As seen in our SEM microscopy images, the low-pressure O_2-plasma exposure changes the morphology of the pristine silver substrate even for exposure times as short as 1 min (see Figure S3 (a−f)), while the clean Pt substrate remains unaffected (Figure S3 (g−i)). Nevertheless, once the Cu dendrites were electrochemically grown on both substrates, the dendrites themselves were found to be surprisingly resistant to morphological changes after short plasma treatment times up to 1 min (see Figure S4) and to CO_2RR conditions for up to 1 h at −0.9 V vs RHE. This picture changes for longer plasma treatment times such as 5 min. Here, a decrease in the sharpness of the dendrite tips (Figure 1 (e,g)) is observed, which results from the formation of CuO, as confirmed by our XPS and EDX measurements (Table S1). Upon exposure to the electrochemical conditions, visible roughening and the presence of small particles on top of the dendrites are observed (Figure 1 (f,h)).

To estimate the change in the roughness of the former samples, capacitance measurements were used.[20,23] The data are shown in Figure S5 and are consistent with our SEM analysis. Upon plasma oxidation prior to CO_2RR, the roughness of both samples increases independently of the substrate used. Nevertheless, the increase is two times higher on the Ag substrate as

DOI: 10.1021/acscatal.9b00483
ACS Catal. 2019, 9, 5496−5502

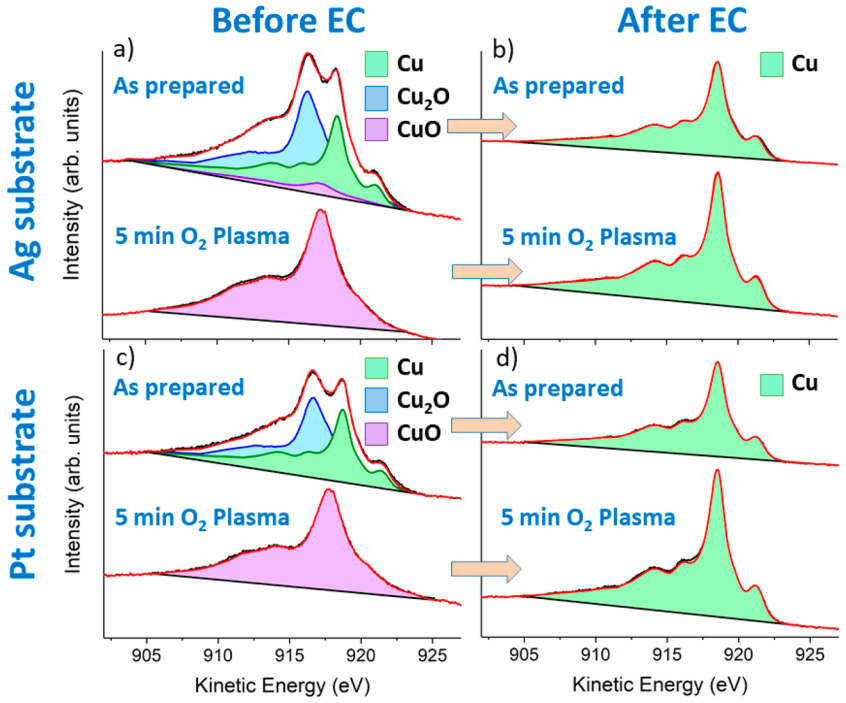

Figure 3. Quasi in situ Cu LMM XPS spectra acquired on Ag- and Pt-supported Cu dendrites before (a, c) and after 1h of CO_2RR at an applied potential of −0.9V vs RHE (b, d). The spectra are fitted with a linear combination of the corresponding Cu, Cu_2O, and CuO reference spectra.

compared to the Pt substrate (see Figure S5). We assigned this difference to the larger changes experienced by the Ag substrate upon O_2-plasma exposure (Figure S3).

The combined faradaic efficiency for the targeted C_2 and C_3 hydrocarbons is shown in Figure 2 (a) together with that of CO (Figure 2 (b)), methane (Figure 2 (c)), the parasitic hydrogen evolution reaction (Figure 2 (d)), and the desired multicarbon products, namely, ethanol (Figure 2 (e)) and ethylene (Figure 2 (f)) (for 1-prop, C_2H_6, and HCOOH, see Figure S6). It is evident that the O_2-plasma pretreatment is able to increase the yield of the desired C2−C3 products by up to 20% at −0.9 V vs RHE, while suppressing hydrogen and methane formation, which has not been demonstrated for these types of samples in the absence of the plasma prefunctionalization. Another important new feature of the present samples is that there is an additional promoting effect on the selectivity toward C_2 and C_3 products depending on the substrate used. In this case, and regardless of the plasma pretreatment, the performance of the dendrites is increased when supported on Ag versus Pt. We attribute this difference to the fact that Ag is able to reduce CO_2 toward CO while Pt is known to be active only for the hydrogen evolution reaction (HER) and not for CO_2RR due to its strong binding to CO that leads to poisoning of the surface.[4] The Ag substrate serves as a source for CO that might be more strongly bound at the rough Cu dendrite/Ag support interface, similar to what has been reported for other gases on these types of interfaces.[34] This might facilitate further CO_2 reduction to C_2−C_3 products.

To gain further insight into the role of the support on CO_2RR, the CO faradaic efficiency of the pristine Ag and Pt substrates must be considered, Figures S8 and S9. Our plasma treated Ag substrate is active for CO_2 reduction toward CO in the entire potential range investigated here for Cu dendrites/Ag, while Pt is only shown to be active for HER but not for CO_2RR. For the Cu/Ag system, 5−10% CO is detected at potentials higher than −0.95 V vs RHE, while no CO is detected for Cu/Pt. This indicates that the CO observed at these high potentials is being produced on exposed Ag substrate areas.[1,23] On the other hand, exposed Pt areas in the Cu/Pt system lead to the observed increase in the hydrogen production above −0.9 V vs RHE.

In Figure 2 (b), it can be seen that the highest CO production at low overpotential (−0.6 V vs RHE) is obtained for the Cu/Ag sample pretreated by a 5 min O_2-plasma. This is assigned to the role of the Ag support, since the pristine plasma-treated Ag foil is up to 70% more selective toward CO in comparison to the untreated one at the same potential due to its enhanced roughness and special defects created during the plasma pretreatment.[10] Therefore, the improved selectivity toward C_2 and C_3 products observed for the Ag-supported Cu dendrites as compared to those grown on Pt is indeed linked to the amount of CO generated by the substrate which, in a coupled reaction mechanism, is able to become further reduced by the dendritic copper overlayer.

Since in the case of the Cu/Pt system the generated CO can only originate from the copper dendrites, the decreased selectivity toward CO upon oxygen plasma treatment suggests the preference of a different pathway, namely, the one leading to C_2−C_3 products (18% increase after O_2-plasma with respect to the as prepared state for potentials as low as −0.7 V vs RHE). In addition, our plasma treatment is able to further reduce the selectivity toward methane for potentials higher than −0.9 V vs RHE in favor of ethylene and ethanol on both substrates. Nevertheless, this additional CH_4 suppression is proportional to the roughness (see Figure S5), which might result in an increased local pH.[34,36] The overall increase in the ethylene and ethanol production can however not be explained by this fact alone, as the increase of up to 20% is already present at potentials as low as −0.9 V vs RHE, while the methane generation is not observed for potentials lower than −0.9 V vs RHE for the as prepared samples on Ag and Pt. Moreover, our plasma treated

DOI: 10.1021/acscatal.9b00483
ACS Catal. 2019, 9, 5496−5502

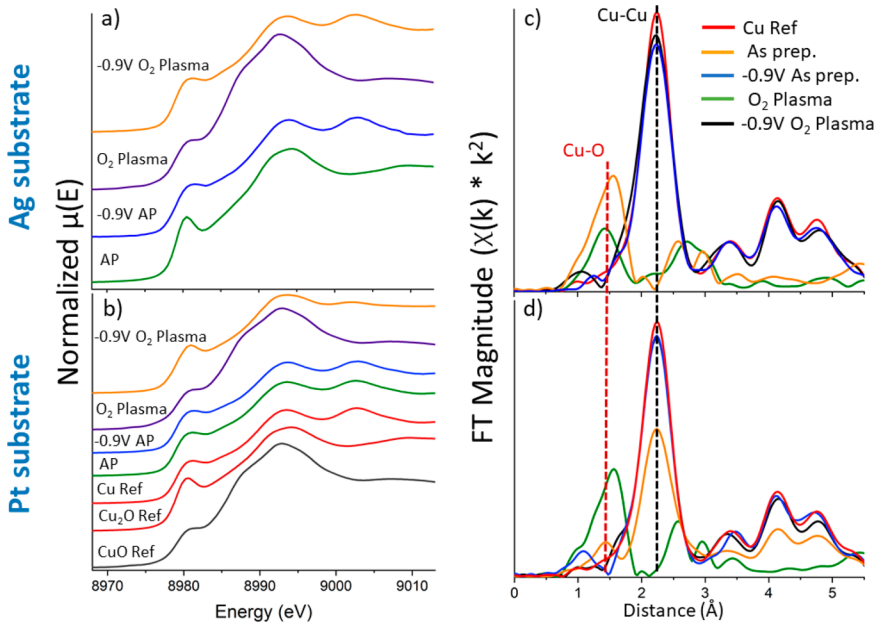

Figure 4. XANES spectra of the as prepared and 5 min O_2-plasma treated Cu dendrite samples supported on (a) Ag and (b) and Pt. The measurements were conducted on the differently pretreated samples before and during CO_2RR at −0.9 V vs RHE. Panels (c) and (d) show the corresponding FT signals in r-space for Cu/Ag and Cu/Pt. Dashed lines indicate the position of the characteristic peaks for Cu−Cu and Cu−O coordination.

samples were found to suppress the unwanted parasitic hydrogen evolution reaction. Thus, we attribute the overall higher partial current density for hydrocarbons on Ag-supported samples as compared to the Pt-supported ones to the further reduction of the CO generated on the exposed areas of the Ag substrate.

To further understand the role of the chemical state of Cu and the surface roughness on CO_2RR activity and selectivity, quasi in situ XPS and operando XAFS measurements of our catalysts were conducted. The results are shown in Figures 3 and 4 as well as in Figure S10 and Table S2 for the Ag substrate, which turns out to be metallic during CO_2RR. As it can be seen from the fitting of the Cu LMM Auger lines with the corresponding reference spectra, all samples contain Cu_xO species before CO_2RR, and the ones O_2-plasma pretreated were found to have fully oxidized CuO surfaces.

On the Cu dendrite samples, the quasi in situ XPS data (Figure 3) revealed that, irrespective of the sample pretreatment, the oxides do not survive during CO_2RR at an applied potential of −0.9 V vs RHE, which is the peak performance potential for ethylene production. Consequently, we do not expect them to be present at even higher potentials (such as −1.0 V or −1.1 V vs RHE), which in fact were found to show a high faradaic efficiency for ethanol and 1-propanol. The improved C_2−C_3 selectivity of these dendritic structures is therefore not linked to the presence of residual Cu_xO during the reaction, as previously discussed in the literature based on ex situ spectroscopic data,[32,45] since they promptly become reduced under reaction conditions, but rather to their rough and defective structure. Additionally, we tested whether Cu_xO species are present directly after the in situ dendritic electrochemical growth and before CO_2RR to shed light into a question raised in the literature[32] on whether the improved C−C coupling observed for these structures could be due to the fact that the dendrites were initially containing Cu_xO and that the subsequent oxide-reduction process could lead to their improved catalytic performance. We therefore grew the dendrites on a commercially available carbon-based gas diffusion electrode (Freudenberg C2 GDL) within our UHV-compatible electrochemical cell and conducted quasi in situ XPS measurements directly after deposition (following the synthesis described in ref 32) and before air exposure. No Cu_xO species were observed directly after deposition (Figure S11). These XPS data corroborate that the better efficiency for C_2 and C_3 products seen for our plasma-pretreated dendrite samples and also for the pristine dendrite samples presented in the literature is not linked to residual Cu oxides remaining during the reaction.

Regarding the role of the needle-like structure, Klingan et al.[36] were able to show that indeed the local pH at the dendrite surface increases, thus favoring the formation of ethylene over methane. That this increase in the selectivity is indeed linked to the needle like structure and not to an overall roughness of the dendrite surface was demonstrated by Reller et al.[32] who reported a clear drop of the selectivity toward ethylene in correlation to a coarsening of the needle-like structures. Although we managed to stabilize this beneficial dendritic structure even upon plasma pretreatment, our catalysts show a worse performance for C−C hydrocarbons as compared to previously published oxide derived catalysts,[23] which is possibly due to the lack of stabilization of Cu(I) within the copper dendrites supported on Ag and Pt as shown by our quasi in situ XPS and operando XAFS.

Since XPS is a surface-sensitive technique and does not provide bulk chemical or structural information, operando XAFS measurements were carried out to confirm the absence of the Cu oxides also under subsurface reaction conditions, Figure 4. It was hypothesized that such oxides could migrate toward the surface during the reaction due to the concentration gradient across the sample and through their progressive reduction lead to a special defective undercoordinated structure that was stable during the reaction. Linear combination fitting (see Table S3) of the XANES data presented in Figure 4 (a,b) reveals that CuO is the dominant species for our plasma treated samples on both substrates before electrochemistry, which is consistent with our

DOI: 10.1021/acscatal.9b00483
ACS Catal. 2019, 9, 5496−5502

XPS analysis (Figure 3), but now, we also demonstrate that it is not only available at the sample surface. Regarding the as prepared Cu dendrites (without plasma exposure) before electrochemistry, a mixture of mainly Cu (53%) and Cu_2O (46%) for the case of the Pt substrate was found while on Ag, the majority of the Cu dendrites are made of Cu_2O (86%). We attribute this to the fact that the samples were exposed to air after their synthesis before the operando CO_2RR XAFS measurements.

Once the potential of −0.9 V vs RHE is applied during CO_2RR, we see almost immediately a change of the XANES spectrum reflecting only the presence of metallic Cu, independently of the initial oxidation state and the substrate used (see Figure 4), as also determined by linear combination fitting. This change can also be clearly seen when looking at the r-space representation of our EXAFS data (Figure 4 (c,d)), as the characteristic peaks for Cu_2O (1.45 Å) and CuO (1.55 Å) vanish during CO_2RR, giving rise to the metallic peak at 2.2 Å, which reflects Cu−Cu coordination. In agreement, our EXAFS fitting analysis shows a Cu−Cu coordination number of N_{Pt} = 10.8−11.3 ± 1.0 for the Pt-supported and N_{Ag} = 11.8 ± 1.5 for the Ag-supported Cu dendrites (see also Table S4). Taking into account the error margins and the fact that the spectra have been corrected for self-absorption, we conclude that our Cu dendrites consist of bulk metallic Cu (N_{Cu-Cu} = 12), which demonstrates that not only the very surface, as probed by XPS, but also the bulk of the sample is metallic during CO_2RR. Thus, Cu_xO species cannot be the active species for the conversion of CO_2 toward hydrocarbons in the dendritic Cu structures. This indicates that the structural properties, especially in the case of the plasma-treated/preoxidized Cu dendrites, are the most important factors determining their CO_2RR performance.

CONCLUSIONS

Our in situ and operando investigation of dendritic Cu electrocatalysts reveals the intricate interplay between structural and chemical characteristics of these materials and their underlying supports with respect to their performance for CO_2 electro-reduction. Here, we were able to improve an already promising CO_2RR catalyst with respect to its selectivity toward ethylene and ethanol by combining the benefits of a low-pressure O_2-plasma treatment leading to an increase of the catalyst surface roughness, with the selection of a suitable support, in this case, Ag, that could serve to increase the CO concentration in the proximity of the Cu catalyst. On such structures, a drastic suppression of the parasitic hydrogen production could be achieved.

Moreover, we were able to demonstrate that the ∼45% faradaic efficiency for C_2−C_3 products obtained is related to structural properties on these materials and not to the presence of residual Cu_xO in the vicinity of the surface or within the bulk as was previously postulated for related oxide-derived Cu catalysts based on ex situ spectroscopic data.

ASSOCIATED CONTENT

Supporting Information

The Supporting Information is available free of charge on the ACS Publications website at DOI: 10.1021/acscatal.9b00483.

Experimental setup for quasi in situ XPS, additional morphological SEM characterization, electrochemical data and measurements, XPS spectra, XAFS quantification, and EXAFS fitting results (PDF)

AUTHOR INFORMATION

Corresponding Author

*E-mail: Roldan@fhi-berlin.mpg.de.

ORCID

Beatriz Roldan Cuenya: 0000-0002-8025-307X

Notes

The authors declare no competing financial interest.

ACKNOWLEDGMENTS

This work was supported by the German Federal Ministry of Education and Research (Bundesministerium für Bildung und Forschung, BMBF) under grants #033RCOO4D-'e-Ethylene' and #03SF0523C-"CO_2EKAT", the European Research Council under grant ERC-OPERANDOCAT (ERC-725915), and the deutsche Forschungsgemeinschaft (DFG) under grant SFB1316, subproject B1.

REFERENCES

(1) Hori, Y.; Murata, A.; Takahashi, R. Formation of Hydrocarbons in the Electrochemical Reduction of Carbon Dioxide at a Copper Electrode in Aqueous Solution. *J. Chem. Soc., Faraday Trans. 1* **1989**, *85*, 2309.

(2) Singh, M. R.; Clark, E. L.; Bell, A. T. Thermodynamic and Achievable Efficiencies for Solar-Driven Electrochemical Reduction of Carbon Dioxide to Transportation Fuels. *Proc. Natl. Acad. Sci. U. S. A.* **2015**, *112*, E6111−E6118.

(3) Graves, C.; Ebbesen, S. D.; Mogensen, M.; Lackner, K. S. Sustainable Hydrocarbon Fuels by Recycling CO_2 and H_2O with Renewable or Nuclear Energy. *Renewable Sustainable Energy Rev.* **2011**, *15*, 1−23.

(4) Hori, Y. *Electrochemical CO_2 Reduction on Metal Electrodes BT - Modern Aspects of Electrochemistry*; Vayenas, C. G., White, R. E., Gamboa-Aldeco, M. E., Eds.; Springer New York: New York, NY, 2008; Vol. *42*; pp 89−189.

(5) Azuma, M. Electrochemical Reduction of Carbon Dioxide on Various Metal Electrodes in Low-Temperature Aqueous $KHCO_3$ Media. *J. Electrochem. Soc.* **1990**, *137*, 1772.

(6) Mistry, H.; Varela, A. S.; Kühl, S.; Strasser, P.; Cuenya, B. R. Nanostructured Electrocatalysts with Tunable Activity and Selectivity. *Nat. Rev. Mater.* **2016**, *1*, 16009.

(7) Kuhl, K. P.; Cave, E. R.; Abram, D. N.; Jaramillo, T. F. New Insights into the Electrochemical Reduction of Carbon Dioxide on Metallic Copper Surfaces. *Energy Environ. Sci.* **2012**, *5*, 7050−7059.

(8) Peterson, A. A.; Abild-Pedersen, F.; Studt, F.; Rossmeisl, J.; Nørskov, J. K. How Copper Catalyzes the Electroreduction of Carbon Dioxide into Hydrocarbon Fuels. *Energy Environ. Sci.* **2010**, *3*, 1311.

(9) Bagger, A.; Ju, W.; Varela, A. S.; Strasser, P.; Rossmeisl, J. Electrochemical CO_2 Reduction: A Classification Problem. *ChemPhysChem* **2017**, *18*, 3266−3273.

(10) Mistry, H.; Choi, Y.-W.; Bagger, A.; Scholten, F.; Bonifacio, C. S.; Sinev, I.; Divins, N. J.; Zegkinoglou, I.; Jeon, H. S.; Kisslinger, K.; Stach, E. A.; Yang, J. C.; Rossmeisl, J.; Roldán Cuenya, B. Enhanced Carbon Dioxide Electroreduction to Carbon Monoxide over Defect-Rich Plasma-Activated Silver Catalysts. *Angew. Chem., Int. Ed.* **2017**, *56*, 11394−11398.

(11) Hatsukade, T.; Kuhl, K. P.; Cave, E. R.; Abram, D. N.; Jaramillo, T. F. Insights into the Electrocatalytic Reduction of CO_2 on Metallic Silver Surfaces. *Phys. Chem. Chem. Phys.* **2014**, *16*, 13814−13819.

(12) Sun, K.; Wu, L.; Qin, W.; Zhou, J.; Hu, Y.; Jiang, Z.; Shen, B.; Wang, Z. Enhanced Electrochemical Reduction of CO_2 to CO on Ag Electrocatalysts with Increased Unoccupied Density of States. *J. Mater. Chem. A* **2016**, *4*, 12616−12623.

(13) Gao, D.; Zhang, Y.; Zhou, Z.; Cai, F.; Zhao, X.; Huang, W.; Li, Y.; Zhu, J.; Liu, P.; Yang, F.; Wang, G.; Bao, X. Enhancing CO_2 Electroreduction with the Metal−Oxide Interface. *J. Am. Chem. Soc.* **2017**, *139*, 5652−5655.

DOI: 10.1021/acscatal.9b00483
ACS Catal. 2019, 9, 5496−5502

(14) Mistry, H.; Reske, R.; Zeng, Z.; Zhao, Z.-J.; Greeley, J.; Strasser, P.; Cuenya, B. R. Exceptional Size-Dependent Activity Enhancement in the Electroreduction of CO_2 over Au Nanoparticles. *J. Am. Chem. Soc.* **2014**, *136*, 16473−16476.
(15) Zhang, W.; Hu, Y.; Ma, L.; Zhu, G.; Wang, Y.; Xue, X.; Chen, R.; Yang, S.; Jin, Z. Progress and Perspective of Electrocatalytic CO_2 Reduction for Renewable Carbonaceous Fuels and Chemicals. *Adv. Sci.* **2018**, *5*, 1700275.
(16) Nie, X.; Esopi, M. R.; Janik, M. J.; Asthagiri, A. Selectivity of CO_2 Reduction on Copper Electrodes: The Role of the Kinetics of Elementary Steps. *Angew. Chem., Int. Ed.* **2013**, *52*, 2459−2462.
(17) Kortlever, R.; Shen, J.; Schouten, K. J. P.; Calle-Vallejo, F.; Koper, M. T. M. Catalysts and Reaction Pathways for the Electrochemical Reduction of Carbon Dioxide. *J. Phys. Chem. Lett.* **2015**, *6*, 4073−4082.
(18) Kim, D.; Resasco, J.; Yu, Y.; Asiri, A. M.; Yang, P. Synergistic Geometric and Electronic Effects for Electrochemical Reduction of Carbon Dioxide Using Gold-Copper Bimetallic Nanoparticles. *Nat. Commun.* **2014**, *5*, 1−8.
(19) Lee, S.; Park, G.; Lee, J. Importance of Ag-Cu Biphasic Boundaries for Selective Electrochemical Reduction of CO_2 to Ethanol. *ACS Catal.* **2017**, *7*, 8594−8604.
(20) Bernal, M.; Bagger, A.; Scholten, F.; Sinev, I.; Bergmann, A.; Ahmadi, M.; Rossmeisl, J.; Cuenya, B. R. CO_2 Electroreduction on Copper-Cobalt Nanoparticles: Size and Composition Effect. *Nano Energy* **2018**, *53*, 27−36.
(21) Gao, D.; Zegkinoglou, I.; Divins, N. J.; Scholten, F.; Sinev, I.; Grosse, P.; Roldan Cuenya, B. Plasma-Activated Copper Nanocube Catalysts for Efficient Carbon Dioxide Electroreduction to Hydrocarbons and Alcohols. *ACS Nano* **2017**, *11*, 4825−4831.
(22) Grosse, P.; Gao, D.; Scholten, F.; Sinev, I.; Mistry, H.; Roldán Cuenya, B. Dynamic Changes in the Structure, Chemical State and Catalytic Selectivity of Cu Nanocubes during CO_2 Electroreduction: Size and Support Effects. *Angew. Chem., Int. Ed.* **2018**, *57*, 6192−6197.
(23) Mistry, H.; Varela, A. S.; Bonifacio, C. S.; Zegkinoglou, I.; Sinev, I.; Choi, Y.-W.; Kisslinger, K.; Stach, E. A.; Yang, J. C.; Strasser, P.; Cuenya, B. R. Highly Selective Plasma-Activated Copper Catalysts for Carbon Dioxide Reduction to Ethylene. *Nat. Commun.* **2016**, *7*, 12123.
(24) Gao, D.; Scholten, F.; Roldan Cuenya, B. Improved CO_2 Electroreduction Performance on Plasma-Activated Cu Catalysts via Electrolyte Design: Halide Effect. *ACS Catal.* **2017**, *7*, 5112−5120.
(25) Resasco, J.; Chen, L. D.; Clark, E.; Tsai, C.; Hahn, C.; Jaramillo, T. F.; Chan, K.; Bell, A. T. Promoter Effects of Alkali Metal Cations on the Electrochemical Reduction of Carbon Dioxide. *J. Am. Chem. Soc.* **2017**, *139*, 11277−11287.
(26) Singh, M. R.; Kwon, Y.; Lum, Y.; Ager, J. W.; Bell, A. T. Hydrolysis of Electrolyte Cations Enhances the Electrochemical Reduction of CO_2 over Ag and Cu. *J. Am. Chem. Soc.* **2016**, *138*, 13006−13012.
(27) Gao, D.; McCrum, I. T.; Deo, S.; Choi, Y. W.; Scholten, F.; Wan, W.; Chen, J. G.; Janik, M. J.; Roldan Cuenya, B. Activity and Selectivity Control in CO_2 Electroreduction to Multicarbon Products over CuOx Catalysts via Electrolyte Design. *ACS Catal.* **2018**, *8*, 10012−10020.
(28) Lum, Y.; Yue, B.; Lobaccaro, P.; Bell, A. T.; Ager, J. W. Optimizing C-C Coupling on Oxide-Derived Copper Catalysts for Electrochemical CO_2 Reduction. *J. Phys. Chem. C* **2017**, *121*, 14191−14203.
(29) Schouten, K. J. P.; Pérez Gallent, E.; Koper, M. T. M. The Influence of PH on the Reduction of CO and CO_2 to Hydrocarbons on Copper Electrodes Dedicated to Professor Kingo Itaya on the Occasion of His 65th Birthday and in Recognition of His Seminal Contributions to Physical Electrochemistry. *J. Electroanal. Chem.* **2014**, *716*, 53−57.
(30) Todoroki, M.; Hara, K.; Kudo, A.; Sakata, T. Electrochemical Reduction of High Pressure CO_2 at Pb, Hg and In Electrodes in an Aqueous $KHCO_3$ Solution. *J. Electroanal. Chem.* **1995**, *394*, 199−203.
(31) Hara, K.; Kudo, a; Sakata, T. Electrochemical CO_2 Reduction on a Glassy Carbon Electrode under High Pressure. *J. Electroanal. Chem.* **1997**, *421*, 1−4.
(32) Reller, C.; Krause, R.; Volkova, E.; Schmid, B.; Neubauer, S.; Rucki, A.; Schuster, M.; Schmid, G. Selective Electroreduction of CO_2 toward Ethylene on Nano Dendritic Copper Catalysts at High Current Density. *Adv. Energy Mater.* **2017**, *7*, 1602114.
(33) Loiudice, A.; Lobaccaro, P.; Kamali, E. A.; Thao, T.; Huang, B. H.; Ager, J. W.; Buonsanti, R. Tailoring Copper Nanocrystals towards C_2 Products in Electrochemical CO_2 Reduction. *Angew. Chem., Int. Ed.* **2016**, *55*, 5789−5792.
(34) Dutta, A.; Rahaman, M.; Mohos, M.; Zanetti, A.; Broekmann, P. Electrochemical CO_2 Conversion Using Skeleton (Sponge) Type of Cu Catalysts. *ACS Catal.* **2017**, *7*, 5431−5437.
(35) Dinh, C. T.; Burdyny, T.; Kibria, G.; Seifitokaldani, A.; Gabardo, C. M.; Pelayo García De Arquer, F.; Kiani, A.; Edwards, J. P.; De Luna, P.; Bushuyev, O. S.; Zou, C.; Bermudez, R. Q.; Pang, Y.; Sinton, D.; Sargent, E. H. CO_2 electroreduction to Ethylene via Hydroxide-Mediated Copper Catalysis at an Abrupt Interface. *Science* **2018**, *360*, 783−787.
(36) Klingan, K.; Kottakkat, T.; Jovanov, Z. P.; Jiang, S.; Pasquini, C.; Scholten, F.; Kubella, P.; Bergmann, A.; Roldan Cuenya, B.; Roth, C.; Dau, H. Reactivity Determinants in Electrodeposited Cu Foams for Electrochemical CO_2 Reduction. *ChemSusChem* **2018**, *11*, 3449−3459.
(37) Ripatti, D. S.; Veltman, T. R.; Kanan, M. W. Carbon Monoxide Gas Diffusion Electrolysis That Produces Concentrated C_2 Products with High Single-Pass Conversion. *Joule* **2019**, *3*, 240−256.
(38) De Luna, P.; Quintero-Bermudez, R.; Dinh, C.-T.; Ross, M. B.; Bushuyev, O. S.; Todorović, P.; Regier, T.; Kelley, S. O.; Yang, P.; Sargent, E. H. Catalyst Electro-Redeposition Controls Morphology and Oxidation State for Selective Carbon Dioxide Reduction. *Nat. Catal.* **2018**, *1*, 103−110.
(39) Hori, Y.; Konishi, H.; Futamura, T.; Murata, A.; Koga, O.; Sakurai, H.; Oguma, K. Deactivation of Copper Electrode" in Electrochemical Reduction of CO_2. *Electrochim. Acta* **2005**, *50*, 5354−5369.
(40) Hall, A. S.; Yoon, Y.; Wuttig, A.; Surendranath, Y. Mesostructure-Induced Selectivity in CO_2 Reduction Catalysis. *J. Am. Chem. Soc.* **2015**, *137*, 14834−14837.
(41) Wuttig, A.; Surendranath, Y. Impurity Ion Complexation Enhances Carbon Dioxide Reduction Catalysis. *ACS Catal.* **2015**, *5*, 4479−4484.
(42) Biesinger, M. C.; Lau, L. W. M.; Gerson, A. R.; Smart, R. S. C. Resolving Surface Chemical States in XPS Analysis of First Row Transition Metals, Oxides and Hydroxides: Sc, Ti, V, Cu and Zn. *Appl. Surf. Sci.* **2010**, *257*, 887−898.
(43) Ravel, B.; Newville, M. ATHENA, ARTEMIS, HEPHAESTUS: Data Analysis for X-Ray Absorption Spectroscopy Using IFEFFIT. *J. Synchrotron Radiat.* **2005**, *12*, 537−541.
(44) Booth, C. H.; Bridges, F. Improved SelfAbsorption Correction for Fluorescence Measurements of Extended X-Ray Absorption Fine Structure. *Phys. Scr.* **2005**, 202.
(45) Dutta, A.; Rahaman, M.; Luedi, N. C.; Mohos, M.; Broekmann, P. Morphology Matters: Tuning the Product Distribution of CO_2 Electroreduction on Oxide-Derived Cu Foam Catalysts. *ACS Catal.* **2016**, *6*, 3804−3814.

DOI: 10.1021/acscatal.9b00483
ACS Catal. 2019, 9, 5496−5502